High-Speed Digital Baseband Mixer

F. P. Chan, M. P. Quirk, and R. F. Jurgens
Communications Systems Research Section

This paper explores the feasibility of designing a digital, complex, baseband mixer with a 50 MHz sampling rate. The baseband filter must provide passbands with linear phase response to minimize intersymbol interference. The article includes studies of the effects of signal quantization, filter coefficient quantization, dynamic range, filter response characteristics, and the performance of the mixer when used for cross-correlation and autocorrelation pulse detection techniques. This filter has been designed for use in the High-Speed Data-Acquisition System (HSDAS), an advanced experimental system in the Deep Space Network.

I. Introduction

A High-Speed Data-Acquisition System (HSDAS) is being constructed at Deep Space Station 14 (Ref. 1). Its primary purpose is to sample the 15 MHz bandwidth intermediate-frequency (IF) signal from the Deep Space Network (DSN) radar receivers and perform all necessary data reduction (filtering, phase correcting, and correlating; see Fig. 1) using digital processors. A particular front-end module in the HSDAS is the digital baseband mixer. Its purpose, similar to that of its analog counterpart, is to down-convert the IF signal to a complex baseband signal. The real and imaginary components of the baseband signal are obtained by first mixing the IF signal with cosine and sine carrier signals and then filtering out the high-order frequency components.

The digital mixer design must satisfy the requirements of the HSDAS specification. Firstly, it must have appropriate phase and magnitude response so that it induces minimum intersymbol interference in radar signal correlation at later stages. Secondly, it must eliminate out-of-band signal components. Finally, the mixer must have sufficient dynamic range that weak signals buried among strong radar echoes can be detected.

This article presents the design and simulation results for a digital mixer which complies with the constraints listed above. Section II, Digital versus Analog, discusses the advantages and the disadvantages of the two implementations. Section III, Digital Design, outlines the basic structure of the mixer system. Section IV, FIR filter design, discusses the implementation of the post-multiplier, finite impulse response (FIR) filter. Section V, Simulation, presents the simulation results for the digital mixer design. Finally, Section VI suggests future research.

II. Digital Versus Analog

Traditionally, frequency down-conversion has been performed by analog mixers. Recent advances in digital signal processing (DSP) techniques and digital hardware technology have made a high-speed digital mixer feasible. A digital approach has a number of inherent advantages. Firstly, the

characteristics of a digital device, such as the frequency response of a digital filter, are known exactly. Secondly, the functional characteristics are not affected by component drift, component aging, and ambient temperature change. Thirdly, a digital device can be replicated precisely. Fourthly, a digital circuit can be debugged exactly by slowing down the system clock so that equipment, such as a state analyzer, can be used to monitor or alter logic values in any data path. Furthermore, a digital system is potentially programmable. This feature is an important advantage over an analog device since the latter must be redesigned for any change in system configuration. Finally, a digital hardware implementation can be simulated accurately. An adequate simulation can predict virtually any system performance or design flaw.

In addition to the inherent advantages listed above, a digital mixer design offers implementation alternatives that are lacking in an analog design. Figure 2(a) shows a typical analog design of one channel of a baseband mixer. The first module is a multiplier, usually implemented with diode-switching techniques. A carrier signal in the form of a square wave drives the switching. The output signal contains not only the fundamental baseband signal but also the odd harmonics across the high-frequency spectrum. A low-pass filter with substantial stopband attenuation must be used to filter out the high-frequency harmonics. Figure 2(b) shows a digital design of the same mixer. The incoming signal is arithmetically multiplied with a carrier signal generated from a sine table. The mixed signal contains a baseband component and a component at twice the carrier frequency. Since the component at twice the carrier frequency is the only component to be filtered, the required stopband attenuation is less than that of the analog version. Moreover, system noise caused by the high-frequency odd harmonics found in the diode-switching implementation are nearly eliminated in the digital design.

An important design consideration is the restriction on the filter characteristics imposed by binary coded signals such as those used for telemetry and ranging systems (for example, delay-Doppler radar). In the delay-Doppler technique (Ref. 2), useful information is extracted by cross-correlating the incoming signal with the previously transmitted binary code. Intersymbol interference in correlation, commonly caused by phase distortion in previous filter stages, must be minimized. Therefore, the lowpass filter in the baseband mixer must have a linear phase response, or equivalently, constant group delay, at least over the baseband spectrum. In addition, the magnitude response must preserve as much baseband signal as possible but must cut off sharply near the carrier frequency to remove the high-order frequency component of the mixed signal. This requirement translates to a narrow transition band if the full baseband channel is to be utilized.

In an analog filter design, the requirement for a small transition band conflicts with the requirement for linear phase. For example, Fig. 3 shows the magnitude and phase responses and the group delay of an inverse Chebyshev filter (Ref. 3), designed with the best compromise of the two requirements. Notice that the group delay degrades significantly near the transition band. In a digital design, however, a non-recursive, finite impulse response (FIR) filter (Ref. 4) can be designed such that its phase response is strictly linear without jeopardizing the width of the transition band. Figure 4 shows the magnitude and phase responses and the group delay of an FIR filter with its magnitude response similar to the analog one in Fig. 3. The linear phase property of the FIR filter is one of the most desirable properties of a digital implementation.

The digital approach does have a number of drawbacks. Although the width of the transition band of an FIR filter is not restricted by the phase response, it is limited by the maximum filter length which can be built. It can be shown that the filter length (or number of taps) required is inversely proportional to the normalized transition-band width (Ref. 5). As a result, the digital mixer implemented with an FIR filter that has narrow transition band can be larger and more costly than the analog version. However, the digital design contains modular structures which could be implemented with Very Large Scale Integration (VLSI) technology. Currently the clock rates for VLSI DSP components are about a factor of 5 too slow for our application. Using these components in a parallel and pipe-lined implementation would require about 400 packages. As clock speeds and complexity increase in the next few years, the number of components could drop to about 50 packages at a size and cost comparable to an analog mixer.

A second drawback with the digital design is its limited dynamic range. In the planetary radar system, it is desirable to have the largest dynamic range possible so that weak radar signals can be detected among strong primary radar echoes. In the analog design, the dynamic range, typically 10^{10}, is limited by thermal noise. On the other hand, in the digital design, the dynamic range is limited by quantization. For an N-bit digital system, the dynamic range is approximately 2^N. In general, a larger dynamic range requires more data bits at the expense of more complex and slower hardware. As a result, the optimal data word size in a digital mixer is a compromise between the desired dynamic range and the hardware complexity.

III. Digital Design

A number of parameters must be defined for the digital mixer. These parameters include the sampling resolution (or

amplitude quantization), the sampling rate, and the post-multiplier filter characteristics.

As discussed before, the sampling resolution is determined by the required input dynamic range. A 40 dB sensitivity for the HSDAS represents a good compromise among quantization variance, expected weak signal strength, and hardware complexity. This dynamic range is anticipated to be large enough for the actual radar experiments and for equipment testing. A 40 dB sensitivity translates to a digital system with 8-bit resolution. As a result, the digital mixer should be designed with an 8-bit basic data word size.

The sampling rate is limited by the Nyquist sampling theorem, which states, "If a continuous, bandwidth-limited signal contains no frequency components higher than f_x, then the original signal can be recovered without distortion if it is sampled at a rate of at least $2f_x$ samples per second" (Ref. 6). If the signal contains energy at rate f higher than f_x, f will be folded back and superposed at frequency $2f_x - f$. This phenomenon is known as aliasing and must be avoided.

The Nyquist sampling theorem imposes two design restrictions on the digital mixer. Firstly, the mixer must operate at a sampling rate at least twice the highest frequency component of the incoming IF signal. Since the IF signal contains components up to 15 MHz, the sampling rate in the mixer must be at least 30 MHz. Secondly, the Nyquist theorem requires that signal energy at frequencies higher than f_x, 15 MHz, should be filtered before the A/D converter in order to avoid aliasing. This filtering is guaranteed by the HSDAS analog receiver.

In theory, a sampling rate of 30 MHz is the absolute minimum rate for the mixer. Additional consideration, however, is given to the post-mixer baud integrator (Fig. 1). The baud integrator (Ref. 7) is required to resample the data so that the HSDAS can track the Doppler shift of the signal. In order to keep the resampling error sufficiently small, a 50 MHz sampling rate for the A/D converter, the digital mixer, and the baud integrator has been established as a desirable design goal.

The characteristics of the post-multiplier, lowpass FIR filter can now be defined. As shown in Fig. 2(b), in order to extract the baseband signal from the output of the multiplier, the FIR lowpass filter must have a stopband beginning at 7.5 MHz. Because the stopband frequency is fixed, the sum of the passband and transition-band widths must be constant. The widening of one band results in the narrowing of the other. As explained in Section II, it is desirable to have the widest passband possible to preserve the baseband signal, yet it must also have the widest transition band possible to minimize the FIR filter size. These two are conflicting requirements. A proper compromise can be found by considering the spectral characteristics of the incoming radar signal.

Usually, the incoming signal from the HSDAS receiver is an IF signal phase modulated by a pseudorandom (PR) code of 0.5 μs baud period. The signal power spectrum of the binary PR code, shown in Fig. 5, can be expressed as,

$$P(\omega) = C \frac{\sin^2\left(\frac{\omega t_b}{2}\right)}{\left(\frac{\omega t_b}{2}\right)^2} \tag{1}$$

where ω is the angular frequency, t_b is the period of one baud, and C is a constant. It can be shown that the main lobe, between $-1/t_b$ and $+1/t_b$, contains 90.2% of the overall signal energy. A filter with its passband frequency set at $-1/t_b$ to $+1/t_b$ (2 MHz for a 0.5 μs baud period) should pass sufficient signal energy to be correlated at later stages. A 2 MHz passband width leaves a 5.5 MHz transition bandwidth. It will be shown in Section IV that this FIR filter can be realized with 19 taps, a reasonable size. Here, the choice of the filter characteristics is somewhat arbitrary, and its final acceptance will be based on the mixer simulation to verify if the cross-correlation function between the mixer output and the original binary pseudorandom code is acceptable.

In summary, the overall mixer is chosen to operate at 50 MHz with 8-bit basic data resolution. The FIR, lowpass filter is preliminarily chosen to have a passband from 0 to 2 MHz, a transition band from 2 MHz to 7.5 MHz, and a stopband from 7.5 MHz up. The stopband must also have an attenuation of at least 40 dB.

IV. FIR Filter Design

Having defined the characteristics of the FIR filter, one needs to generate the necessary FIR filter coefficients. A number of methods, such as windowing and iteration techniques, have been published (Ref. 8). In this digital mixer design, a computer-aided method based on the equiripple iteration algorithm is employed to determine the optimal FIR filter coefficients.

The time domain filter response for an FIR filter can be viewed as a discrete time approximation of the convolution integral, summed over finite duration (starting from $n = 0$ for a causal system),

$$y(i) = \sum_{n=0}^{N-1} h(n)\, x(i-n) \tag{2}$$

where $h(n)$ is the FIR filter coefficient, $x(n)$ is the input signal, and $y(n)$ is the output signal. The frequency response of an FIR filter having coefficients $h(n)$ and length N can be described as,

$$H(f) = \sum_{n=0}^{N-1} h(n) \exp\left[-j\, 2\pi\, (nf/f_s)\right] \tag{3}$$

where f_s is the sampling frequency. If the following restriction,

$$h(n) = h\,(N-n-1) \tag{4}$$

is imposed on the FIR filter coefficients, the filter has linear phase response (Ref. 9). Furthermore, if the filter has odd length, then the group delay, t_g, is an integer multiple of the sampling period depending only on N,

$$t_g = \left(\frac{N-1}{2}\right) t_s \tag{5}$$

where t_s is the sampling period.

Equation (4) suggests that the FIR filter coefficients are symmetrical about the central coefficient (assuming odd filter length). This is an important fact because it implies that the number of hardware multipliers can be halved by first factoring out identical coefficients.

To find the optimal FIR coefficients, one must first define what the "optimal" filter characteristics are. As mentioned before, it is desirable to minimize the filter length, N, and maximize the width of the passband ω_p (Fig. 6). For a fixed stopband edge, maximizing the passband width is equivalent to minimizing the width of the transition band. In addition, δ_p, the maximum ripple deviation from the ideal passband response of unity, and δ_s, the maximum ripple deviation from the ideal stopband response of zero should be minimized. Minimizing the stopband ripple is equivalent to maximizing the stopband attenuation. Not all of these parameters, N, δ_p, δ_s, ω_p, and ω_s, are independent. In particular, a narrower transition-band width or a larger stopband attenuation typically requires a longer filter length. Parks and McClellan (Ref. 10) have written an iterative algorithm to design symmetric (and antisymmetric) equiripple FIR filters.

This iterative algorithm for finding $h(n)$ involves solving a Chebyshev approximation problem which minimizes the maximum approximation error, ϵ. Specifically, one minimizes, over all sets of N coefficients $h(n)$, the maximum of the absolute value of the weighted difference between the desired frequency response, $D(f)$, and the actual filter response, $H(f)$, for the regions of approximation,

$$\epsilon = \min\,\{\max\,[W(f)\,|\,D(f) - H(f)\,|]\} \tag{6}$$

The weighting function $W(f)$ allows for different relative errors in different bands, and can be used to shape the passband and the stopband.

In the case of the baseband mixer FIR filter, the stopband attenuation has been specified at 40 dB. The following procedure is used to obtain the minimum value of N and the associated filter coefficients, $h(n)$.

(1) Choose an approximate filter length N. The number of coefficients, N, is inversely proportional to the normalized transition-band width,

$$N \approx \frac{C}{f_t/f_s} \tag{7}$$

where f_t is the transition-band width, f_s is the sampling rate, and C is a constant between 1 and 4 and depends on the desired stopband and passband ripples (Ref. 5). A good approximation is to simply choose C equal to 4.

(2) Use the Parks-McClellan algorithm to find the stopband attenuation and the associated filter coefficients.

(3) If the computed stopband attenuation is significantly larger than the desired stopband attenuation, decrease N and return to step 2. If the result is smaller than the desired attenuation, increase N and return to step 2. When the result is just larger than the desired attenuation, the filter has been optimized for minimum N, and the proper filter coefficients, $h(n)$, have been found.

Using the procedure outlined above, a 19-tap FIR filter has been designed to the specifications listed in Section III. Quantized to 8-bit integers, the nineteen FIR filter coefficients are -6, -10, -13, -9, 5, 30, 62, 95, 119, 128, 119, 95, 62, 30, 5, -9, -13, -10, -6. Figure 7 shows the plots of the filter coefficients $h(n)$, the magnitude response (in log scale and in linear scale), and the phase response. Since the filter coefficients $h(n)$ are chosen to be symmetrical, the phase response, as predicted, is linear. From the magnitude response, one observes that the signal rolls off at 2 MHz, reaches -3 dB at about 3.8 MHz, and drops below -40 dB at 7.5 MHz and beyond.

It should be pointed out that the FIR filter hardware constrains only the length of the filter. Within a given filter length, the filter characteristics can be changed simply by reentering a new set of coefficients. Consequently, an FIR filter is programmable. Furthermore, an FIR filter can be, at least in

principle, extended by concatenating additional stages. Thus, a digital FIR filter is a highly flexible filter implementation.

V. Simulation

There are many reasons for a complete simulation of the digital mixer. The principal concern is that, with real radar signal inputs, the mixer must produce a baseband signal that correlates properly with the binary pseuorandom code. One wishes to determine how much the digital mixer will distort the ideal cross-correlation function. In theory, there are two types of errors: intersymbol interference and quantization error. In an analog design, the intersymbol interference will be the main source of distortion because an analog mixer always has a non-linear phase response. In a digital design, on the other hand, the quantization error is likely to be the dominant source of distortion. Through a complete simulation of the digital mixer, one can quantitatively measure the overall quantization error.

A second concern is whether the minimum length filter will provide sufficient stopband attenuation if the FIR filter is operating with fully quantized arithmetic. Furthermore, it must be verified that the 2 MHz passband width is large enough to generate the proper correlation signal. Again, these characteristics can be checked only with a simulation of the hardware. Finally, one would like to determine the minimum signal-to-noise ratio (SNR) of the radar signal in which the pseudorandom code can be detected both by autocorrelation and by cross-correlation methods.

The scope of the baseband mixer simulation is shown in Fig. 8. There are two types of hardware simulated: the active components, such as FIR filters, and the observational components, such as power spectrum display. Figure 8 shows all the active components in rectangular blocks or large circles and all the observational components in small circles.

The active components can be divided into three groups: the source-signal generator, the baseband mixer, and the cross-correlator. The source-signal generator includes a binary pseudorandom code generator, a square-wave generator, an IF radar signal generator, and an analog-to-digital converter. The source-signal generator is responsible for simulating a radar IF signal, phase modulated with either a binary pseudorandom code or a square wave. Complex white noise is added to the IF signal to simulate various SNRs. The source signal can be characterized as,

$$\begin{aligned} \bar{S}(t) &= \bar{N}(t) + \bar{\Gamma} \exp\{j[\omega_c t + \phi(t)]\} \\ \bar{\Gamma} &= \gamma + j0 \end{aligned} \tag{8}$$

where $\bar{N}(t)$ is the complex white noise, γ is the SNR, ω_c is the angular carrier frequency, and $\phi(t)$ is the phase function (either a square wave or a binary pseudorandom code). The real component of $\bar{S}(t)$ is first quantized through an analog-to-digital converter and then sent to the input of the mixer.

The baseband mixer has two channels, one for the real signal and one for the imaginary signal. The mixer consists of three parts: the arithmetic multipliers, the FIR filters, and the optional down-samplers. The incoming IF signal is first arithmetically multiplied with a cosine carrier signal in the real channel and with a sine carrier signal in the imaginary channel. The resulting signals are then filtered through two identical lowpass FIR filters. The output signals from the filters are the baseband complex signal. If one desires, the sampling rate can be reduced by down-sampling the baseband signal. (This option is not used in the present mixer design.)

If the pseudorandom code is used to phase modulate the IF signal, the output channels from the baseband mixer can be fed into two cross-correlators, in which the mixer outputs are correlated with the original binary pseudorandom code.

There are five types of observational components: the time-domain display, the frequency-domain display, the power spectrum display, the autocorrelation display, and the cross-correlation display. The time-domain display shows the two signals in the real and imaginary channels in the time domain. The frequency-domain display shows the magnitude (in dB) of the Fast Fourier Transform (FFT) of the real channel and the FFT of the imaginary channel. The power spectrum display is the magnitude square of the FFT of the complex output signal. The autocorrelation function is then derived by computing the inverse FFT of the power spectrum. Finally, the cross-correlation function is computed by directly correlating two time domain signals. These observational components provide the means with which one can closely examine the characteristics of the signals throughout the system.

The exact simulation of a particular mixer design is determined by a number of user-defined options and parameters. Some of these options and parameters control the characteristics of the source signal, while others control the quantization on the signal paths. The user provides the FIR filter coefficients and the pseudorandom code externally. In addition, the simulation provides an optional signal averaging facility with which the radar signal can be integrated while the random noise is averaged out. Table 1 is a list of parameters chosen for the current mixer design.

Figure 9 shows the results from a typical simulation with an SNR of 10 dB and with no signal averaging. Figure 9(a) shows

the frequency-domain plot of the quantized source signal. The spectrum of the pseudorandom signal is centered about the carrier frequencies at +7.5 MHz and -7.5 MHz. Figures 9(b) and 9(c) show the frequency-domain signals of the real and imaginary channels following multiplication by the cosine and sine carriers. By coincidence, the IF signal phase is lined up with the carrier signal phase such that the output signal energy concentrates solely in the imaginary channel. Generally this would not be true. The IF signals are shifted down to the baseband while the twice-carrier frequency components are also created. Figure 10 shows the FIR filter output signals. The twice-carrier frequency components have been suppressed, leaving only the baseband signals.

Figure 11(a) shows the power spectrum of the complex filter output. The magnitude ratio of the signal peak within the baseband to the noise beyond the baseband is at least 40 dB, as required in the mixer specification. The small lump of signal energy at 15 MHz is the remnant of the original carrier signal.

Figure 11(b) shows the autocorrelation of the radar signal from the mixer. As stated before, the autocorrelation is found by computing an inverse FFT of 2048 frequency samples from the power spectrum (Fig. 10). In this particular plot, the signal has been averaged 16 times. The principal triangular match signal is well defined at time zero. Two smaller triangular match signals exist at time +9.46 μs and -9.46 μs. They are caused by the fact that the 63 baud-long pseudorandom code has a period significantly shorter than the FFT time frame. Since the pseudorandom code period (1575 time samples) is 473 samples short of one FFT time frame (2^{11} or 2048 time samples), the pseudorandom code matches itself again at sample +473 (+9.46 μs) and -473 (-9.46 μs). As a result, the two small signal peaks are artifacts of the way the autocorrelation is computed. They would not occur in an actual implementation.

Figure 12 shows the cross-correlation between the mixer output and the binary pseudorandom code. This plot is generated with no signal averaging. Since the correlation is done in the time domain with exactly one pseudorandom code length, it has no multiple match signals as found in Fig. 11. The match signal is found only in the imaginary channel, a fact consistent with the result from Fig. 9. The match signal is negative because the mixer demodulates the IF signal into an inverse of the original binary pseudorandom code. Furthermore, the peak of the correlation function is found at the 9th time sample because the FIR filter introduced a group delay of 9 sample periods (Eq. [5]) relative to the original binary pseudorandom code.

The cross-correlation function shows a triangular match signal that has no significant distortion from an ideal triangular shape. This result verifies that a 2 MHz filter passband width is sufficient to generate a clean correlation function. Furthermore, the match signal has a peak magnitude defined well above that of the out-of-match correlation noise. No significant intersymbol interference is found. This observation is further supported by the correlation function shown in Fig. 13 where the correlation signal has been avareged 16 times. The out-of-match correlation signal level is held almost perfectly constant. In conclusion, the intersymbol interference, commonly found in an analog system, is almost nonexistent in this digital system.

The relative quantization noise of the overall mixer is evaluated by comparing the cross-correlation function generated by an 8-bit system with that generated by a 30-bit system. The root-mean-square quantization noise level, relative to match signal peak, is found to be -41 dB. Since the quantization noise is below -40 dB, the dynamic range requirement is satisfied.

The effects of a small SNR have also been investigated. In the autocorrelation mode, the pseudorandom code is detectable down to an SNR of 4.7 dB. Below that level, the lowpass characteristics of the FIR filter dominate the autocorrelation signal. In the cross-correlation mode, the pseudorandom code is detectable down to an arbitrarily small SNR provided that enough signal averaging is done to integrate the radar signal and to remove the random noise. It has been verified that the cross-correlation can clearly detect a radar signal down to an SNR ratio of -20 dB by averaging the cross-correlation signal 1600 times.

In summary, the simulation of the digital baseband mixer has verified that the present design meets all specifications. In particular, the current FIR filter generates acceptable cross-correlation functions. There is no significant intersymbol interference detected. The quantization noise is -41 dB relative to the maximum correlation signal. Finally, it is verified that cross-correlation can detect a radar signal with small SNR.

VI. Conclusion

The simulation has shown that an all-digital baseband mixer can satisfy all requirements specified by the High-Speed Data-Acquisition System. The digital mixer has a number of desirable properties, such as stability, programmability, and linear phase response. Furthermore, it has been demonstrated that

a digital mixer generates negligible intersymbol interference in cross-correlation. These very desirable features can not be realized by an analog design. The remaining question is whether the digital mixer can be built with available hardware technology.

With regard to the implementation of the digital mixer, two difficulties exist: It must operate at high speed, and it must be within practical limits in complexity. The digital mixer for the HSDAS must operate at 50 MHz. All digital operations within the mixer, such as multiplying and adding, will be pipelined for synchronous operations. Some parallel processing at lower pipeline clock rates may be necessary. At the present time, the only digital technology that can operate reliably at this speed is the emitter-coupled logic (ECL). One problem associated with ECL is its low logic complexity per chip. To fully implement the logic functions of a digital mixer, a large number of ECL components will be required. To appreciate the complexity problem, one may consider the FIR filter alone. One 19-tap FIR filter as designed in Section IV requires nine 8-X-8-bit multipliers, nineteen 8- to 20-bit adders, and over thirty-eight 8- to 20-bit buffers. In addition, the complex mixer has two filters; thus, the part count doubles. Of course, this has not yet included the carrier signal multipliers and the control logic.

At the present time, this baseband mixer implementation using ECL is considered marginally practical to build. Certainly, the FIR filter length cannot be extended much beyond the present design of 19 taps. However, because of the regular structure of an FIR filter, part of the filter can be implemented with VLSI. The present constraint in this approach is the slow speed (about 20 MHz) of the silicon VLSI technology. In the future, when gallium-arsenide VLSI technology becomes available, 50 MHz FIR filter modules can be built. These VLSI modules can reduce the component count of the baseband mixer considerably.

The Ground Based Radar Astronomy Group anticipates that four identical digital mixers will be built for the HSDAS by 1986. The first step is to construct a prototype so the mixer can be evaluted and adjusted (via programming) in the actual operating environment at DSS 14, Goldstone, California. The simulation results give reasonable assurance that the prototype will operate close to the HSDAS specifications. Programmability of the mixer provides further flexibility since the digital mixer can be fine-tuned to the system requirements. In conclusion, an all-digital high-speed baseband mixer for the HSDAS should be built to take advantage of the digital system performance.

References

1. Deutsch, L. J., Jurgens, R. F., and Brokl, S. S., "The Goldstone R/D High Speed Data Acquisition System," *TDA Progress Report 42-77*, 1984, Jet Propulsion Laboratory, Pasadena, Calif., pp. 87-96.

2. Jurgens, R. F., Goldstein, R. M., Rumsey, H. R., and Green, R. R, "Images of Venus by Three-Station Radar Interferometry – 1977 Results," *Journal of Geophysical Research*, Vol. 85, No. A13, Dec. 30, 1980, pp. 8282-8283.

3. Rabiner, L. R. and Gold, B., *Theory and Application of Digital Signal Processing*, Prentice-Hall, 1975, pp. 230-236.

4. Oppenheim, A. V., and Schafer, R. W., *Digital Signal Processing*, Prentice-Hall, 1975, pp. 155-156.

5. Mintzer, F., and Liu, B., "Practical Design Rules for Optimum FIR Bandpass Digital Filters," *IEEE Trans., Acoust., Speech, Signal Processing*, Vol. ASSP-27, Apr. 1979, pp. 204-206.

6. Zuch, Eugene L., "Principles of Data Acquisition and Conversion," *Data Acquisition and Conversion Handbook*, Datel Intersil, 1982, p. 7.

7. Farazian, K. H., and Jurgens, R. F., "Programmable Digital Baud Integrators for the Radar High-Speed Data Acquisition System," *TDA Progress Report 42-79*, 1984, Jet Propulsion Laboratory, Pasadena, Calif., pp. 142-151.

8. Oppenheim, A. V., and Schafer, R. W., *Digital Signal Processing*, Prentice-Hall, 1975, pp. 239-268.

9. Rabiner, L. R., and Gold, B. *Theory and Application of Digital Signal Processing*, Prentice-Hall, 1975, pp. 77-81.

10. McClellan, J. H., Parks, T. W., and Rabiner, L. R., "FIR Linear Phase Filter Design Program," *Programs for Digital Signal Processing*, IEEE Press, 1979.

Table 1. Parameters of current mixer design

Parameters	Value
Source Signal Parameters:	
(1) Carrier Frequency:	7.50 MHz
(2) Baud Period:	0.50 μs
(3) Binary Phase 0:	$-\pi/2$
(4) Binary Phase 1:	$+\pi/2$
(5) Sampling Frequency:	50.00 MHz
(6) Number of Samples per FFT:	2048
(7) Pseudorandom Code Length:	63 bits
Data Length on Signal Path:	
(1) Source Signal to Multiplier:	8 bits
(2) Carrier Signal to Multiplier:	8 bits
(3) Multiplier to FIR Filter:	8 bits
(4) FIR Filter to Correlator:	8 bits
FIR Filter Configuration:	
(1) Filter Length:	19 taps
(2) Coefficient Bit Length:	8 bits
(3) Product Bit Length:	16 bits
(4) Coefficients:	-6, -10, -13, -9, 5, 30, 62, 95, 119, 128, 119, 95, 62, 30, 5, -9, -13, -10, -6
(5) Filter gain:	0.40 dB
Down Sampling:	none

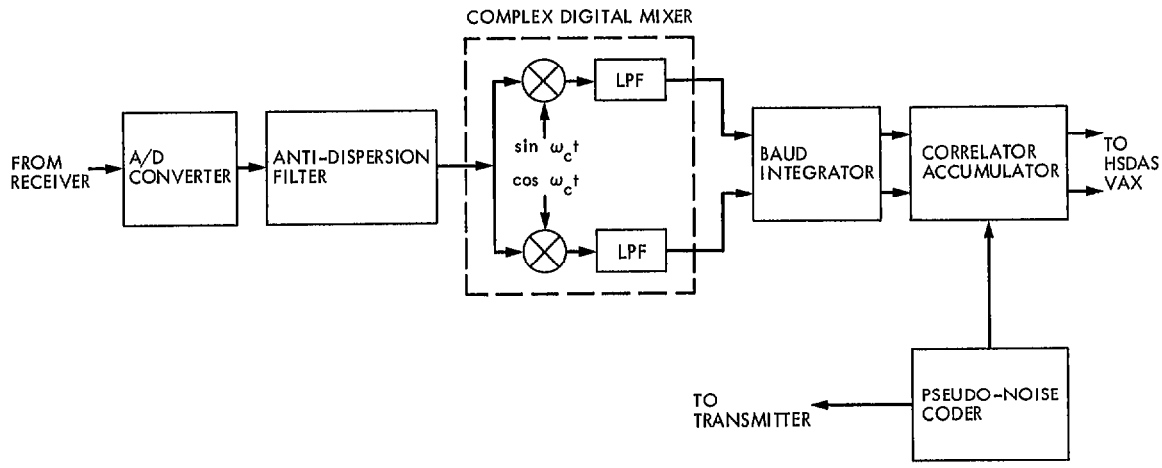

Fig. 1. Simplified block diagram of the HSDAS front end hardware

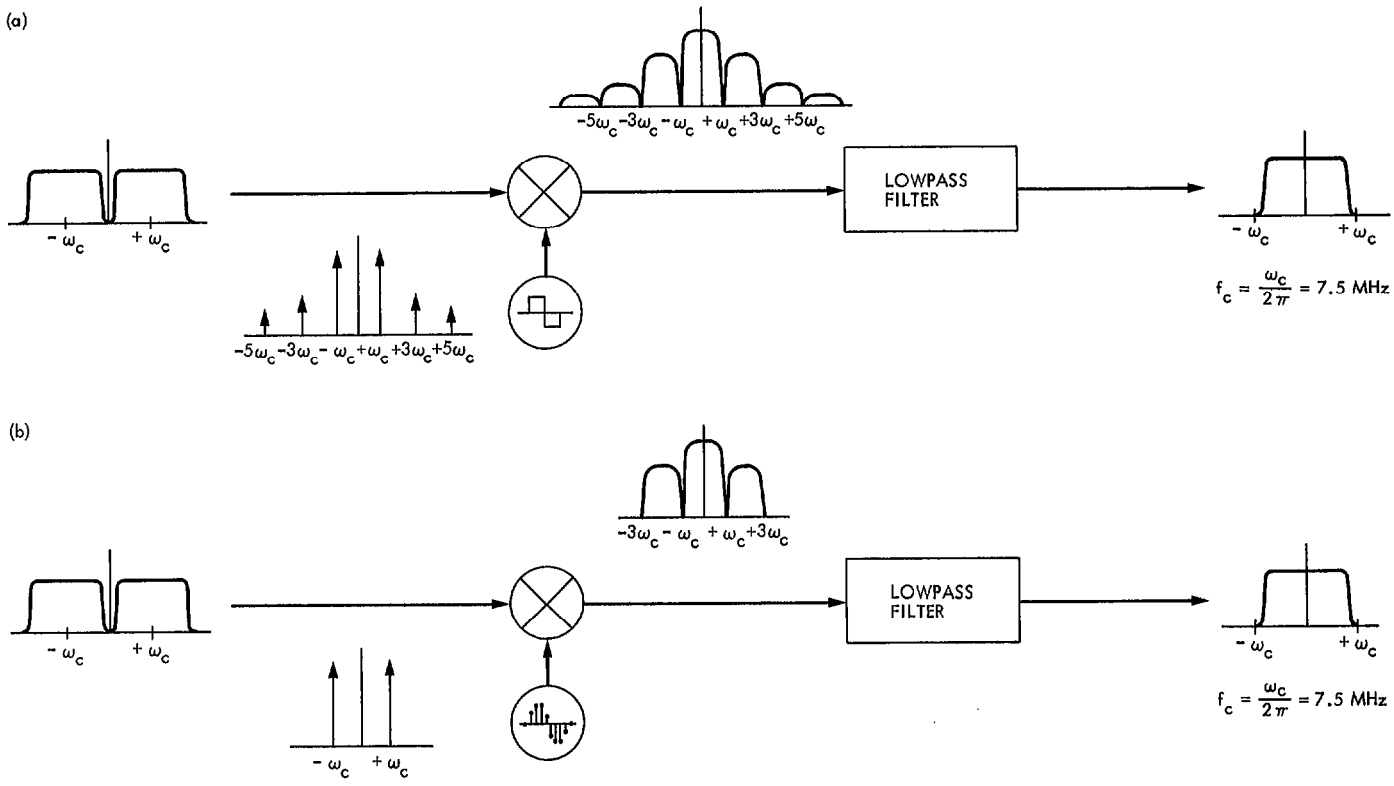

Fig. 2. Signal spectra: (a) analog baseband mixer and signal spectrum; (b) digital baseband mixer and signal spectrum

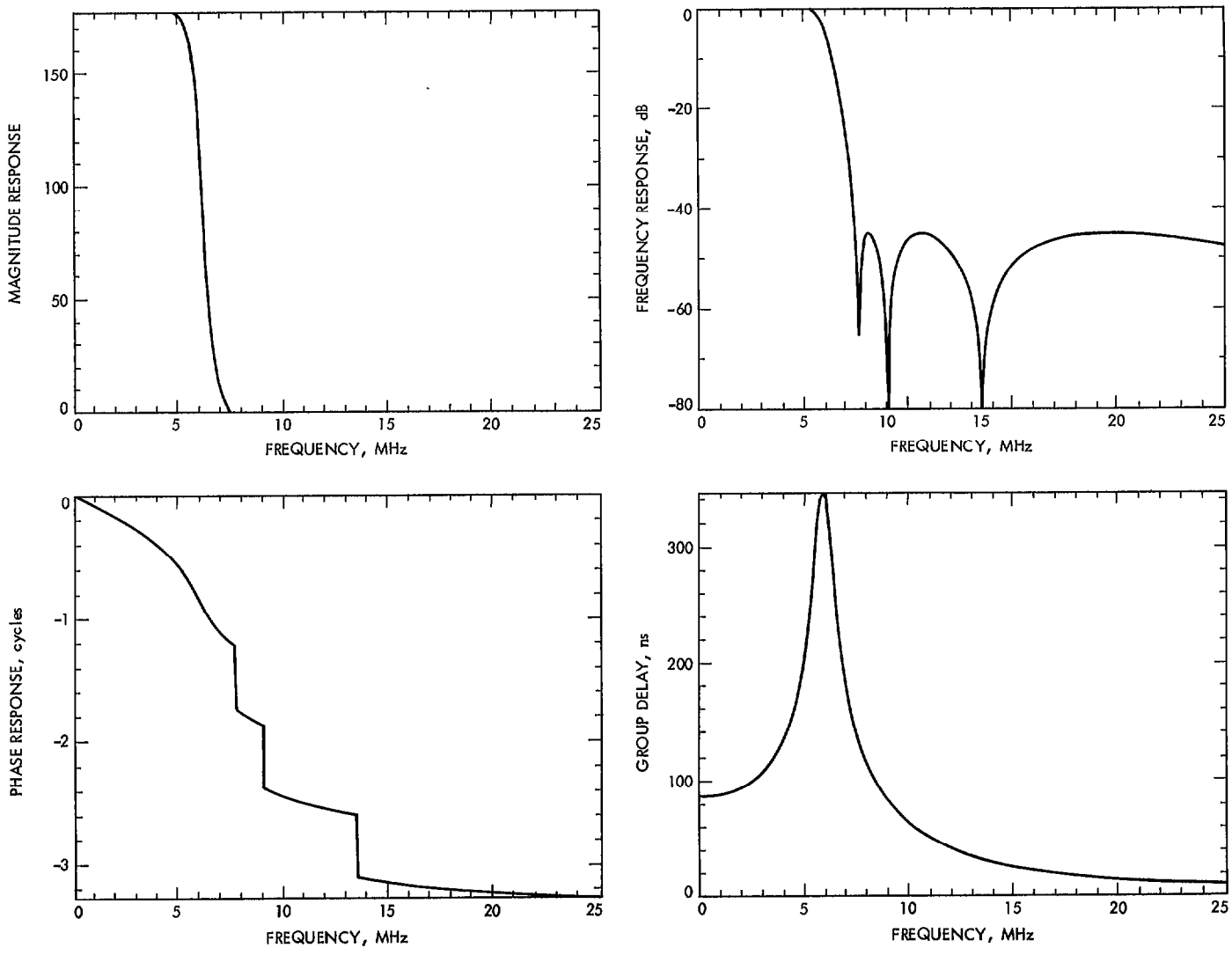

Fig. 3. Analog filter: 8th-order inverse Chebyshev

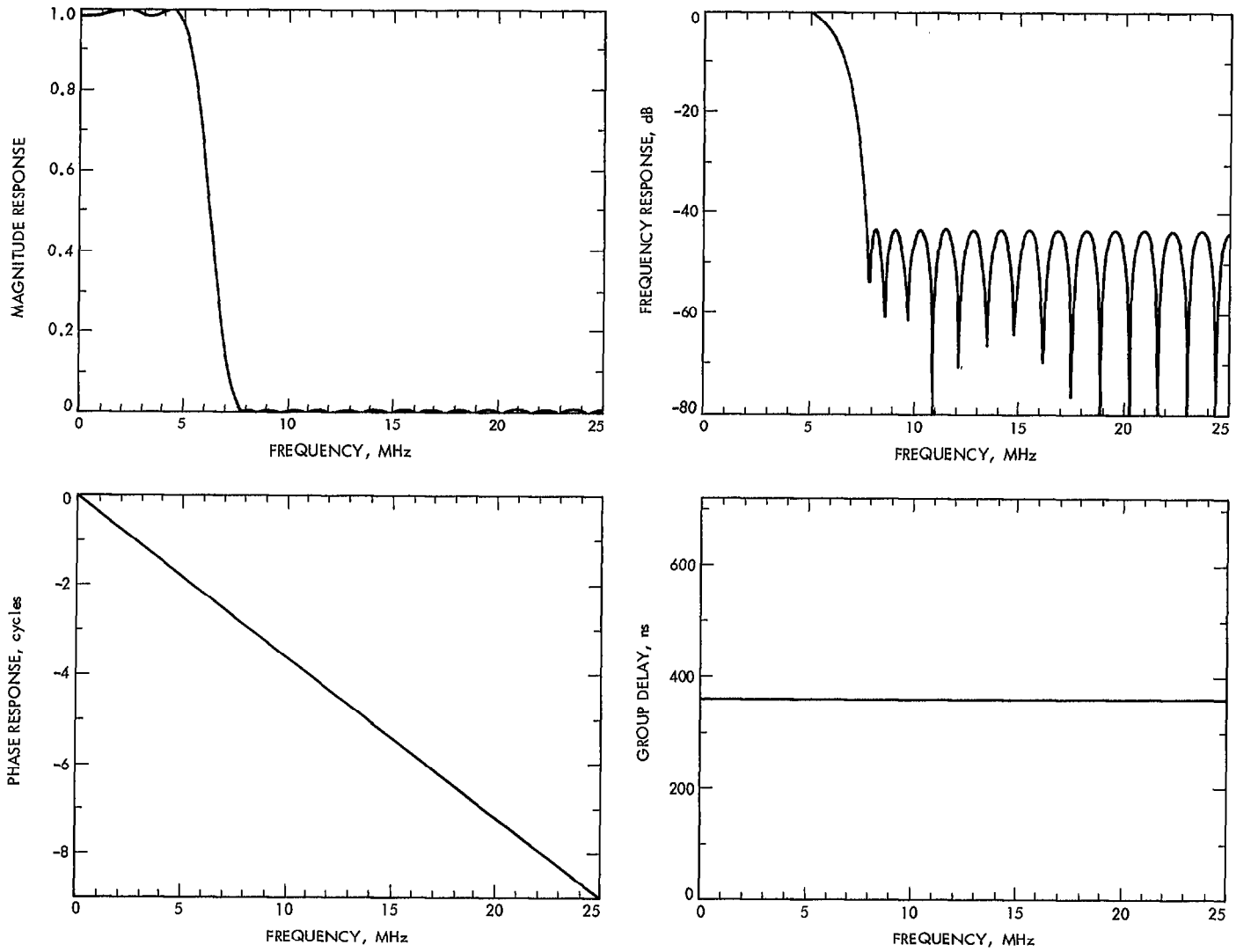

Fig. 4. Digital filter: 37-tap FIR filter

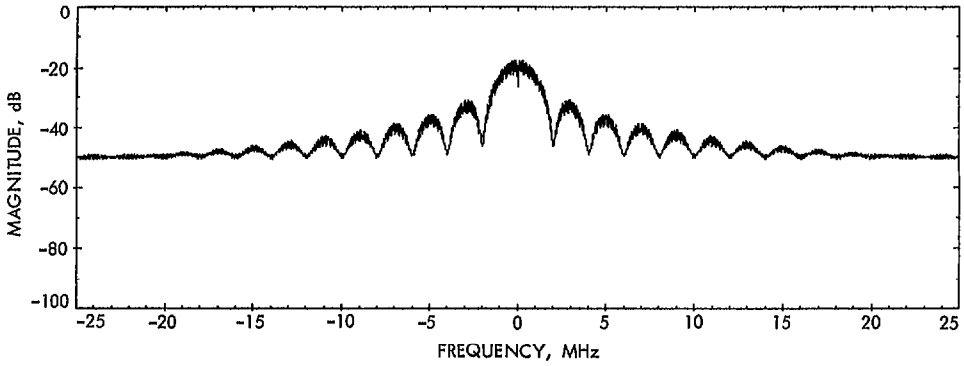

Fig. 5. Power spectrum of a binary pseudorandom code with 0.5 μs baud period

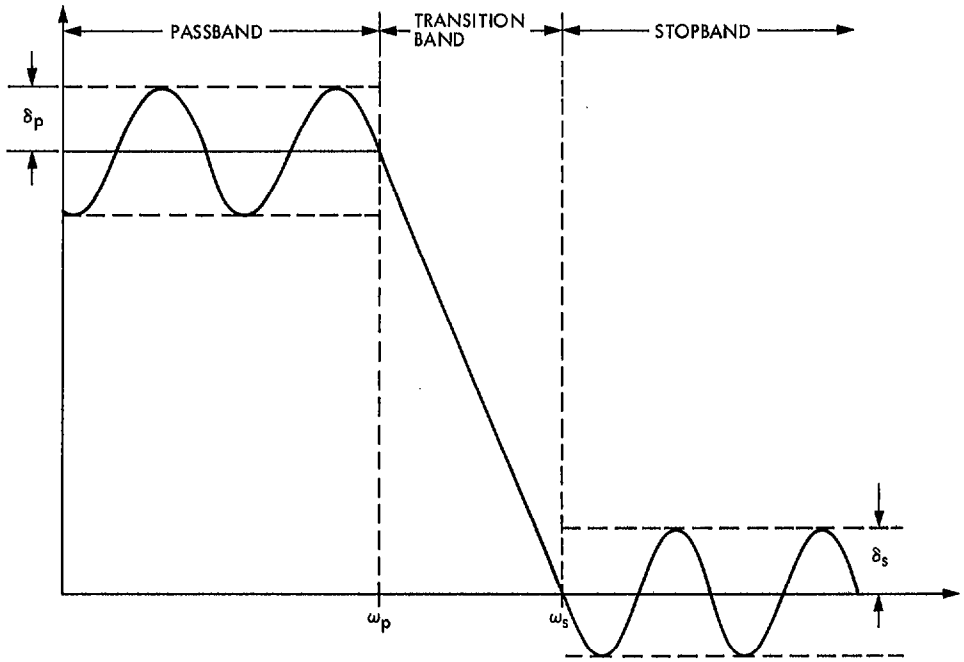

Fig. 6. Parameters of a lowpass FIR filter

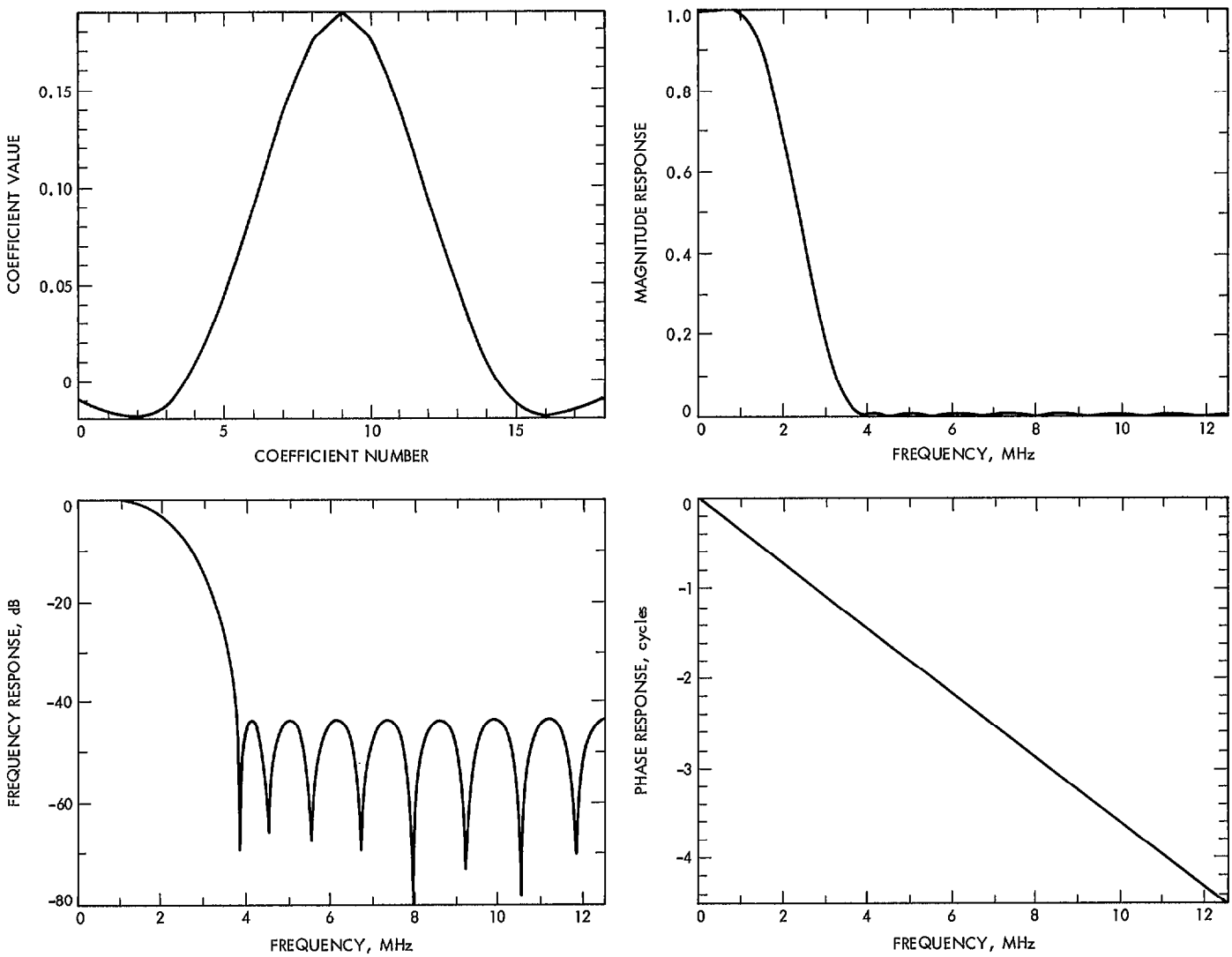

Fig. 7. The 19-tap FIR filter for the digital mixer

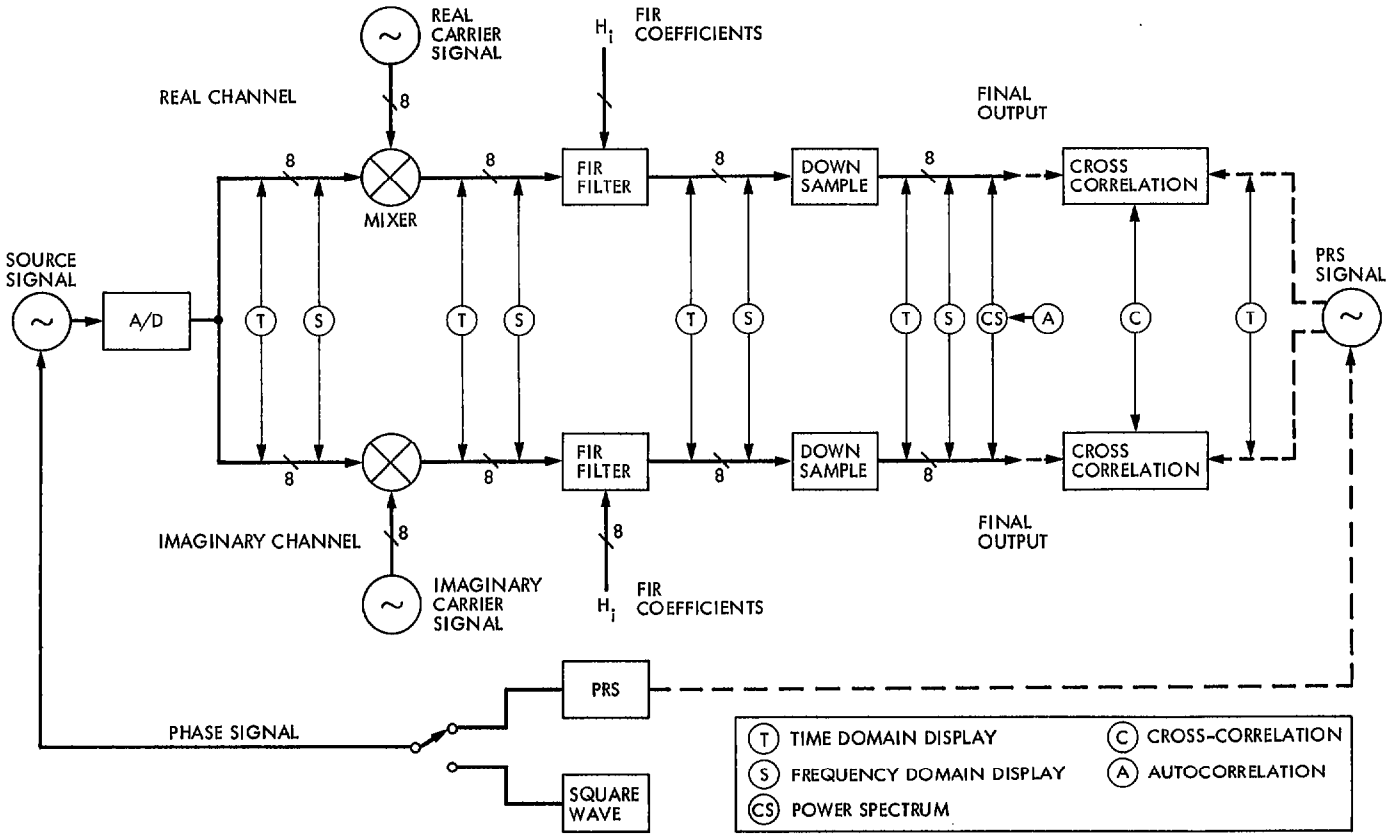

Fig. 8. Baseband mixer simulation block diagram

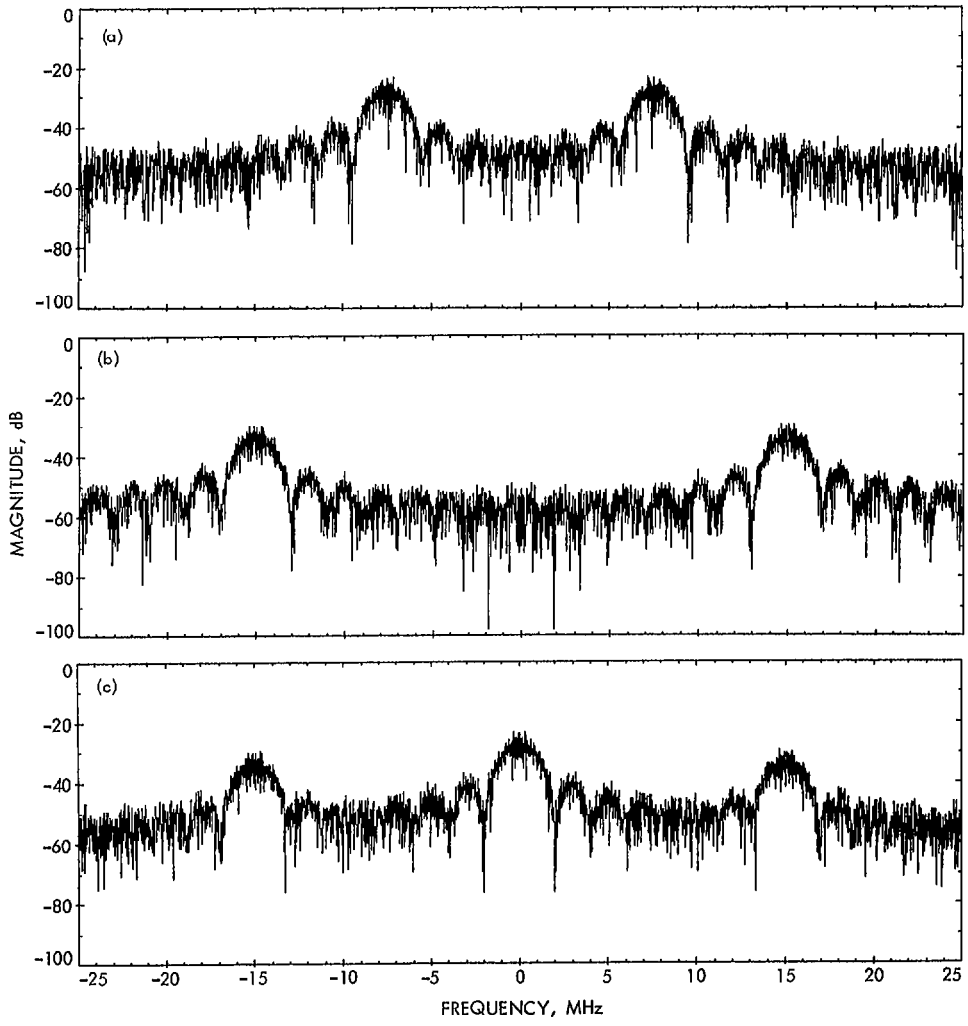

Fig. 9. Simulation results—source and mixer output spectra: (a) source signal frequency spectrum; (b) real channel, multiplier output spectrum; (c) imaginary channel, multiplier output spectrum

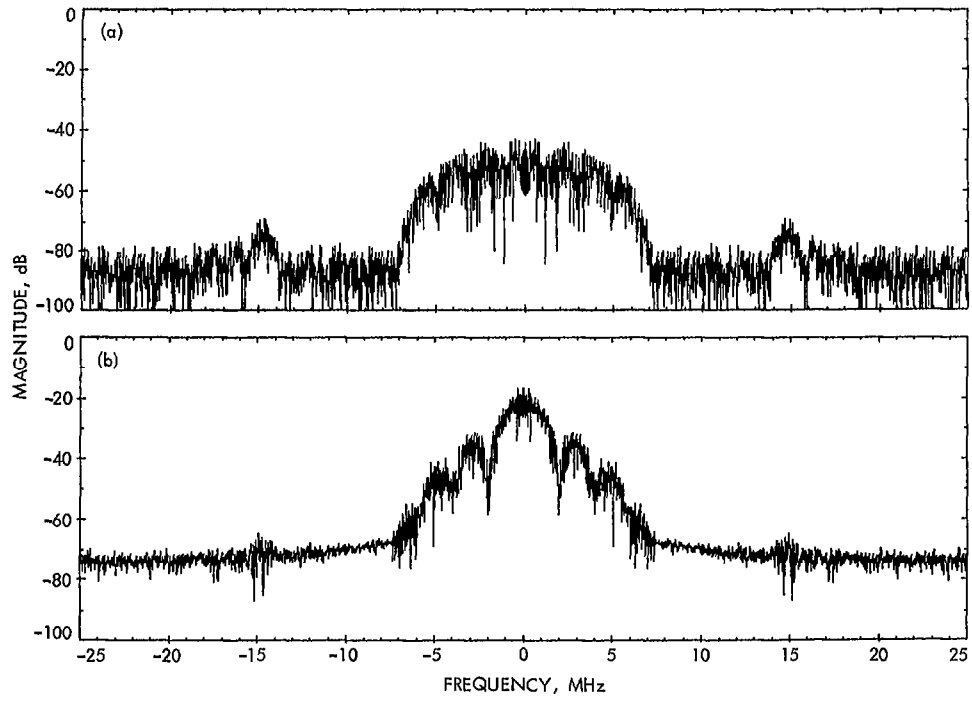

Fig. 10. Filter output spectra: (a) real channel; (b) imaginary channel

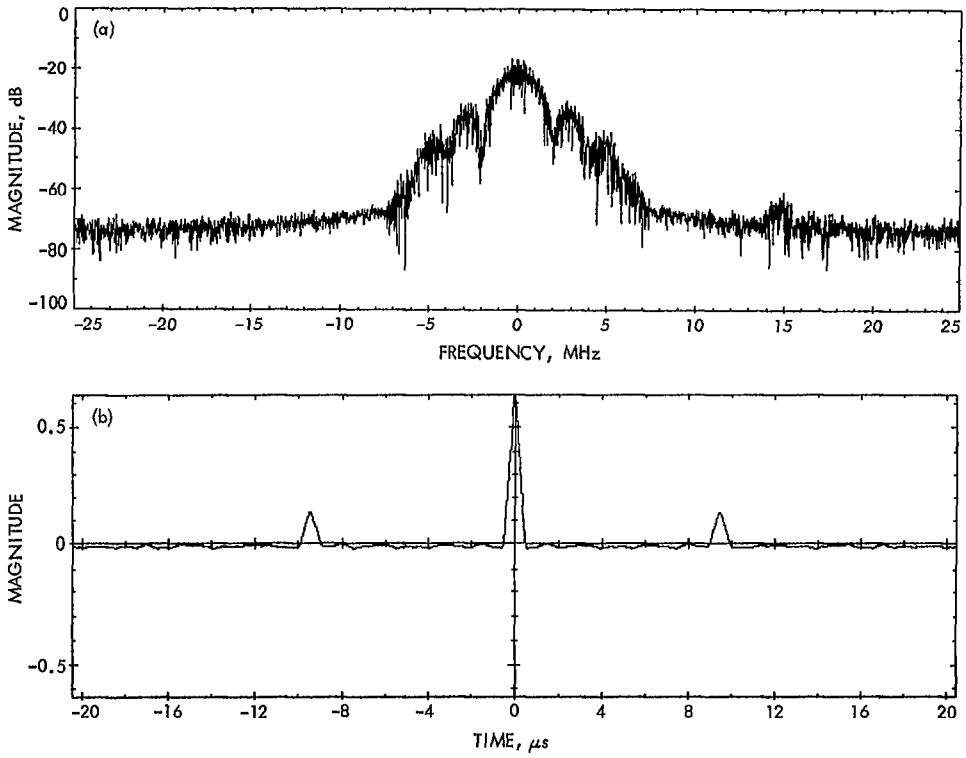

Fig. 11. Mixer output power spectrum and autocorrelation function: (a) power spectrum; (b) autocorrelation

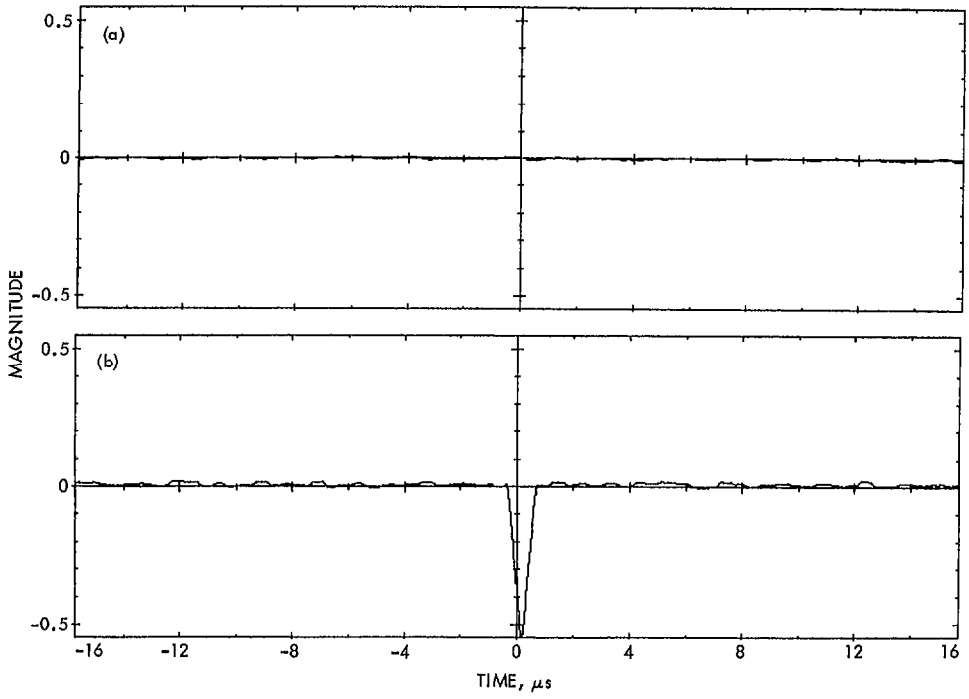

Fig. 12. Cross correlation functions, no signal averaging: (a) real channel, cross correlation; (b) imaginary channel, cross correlation

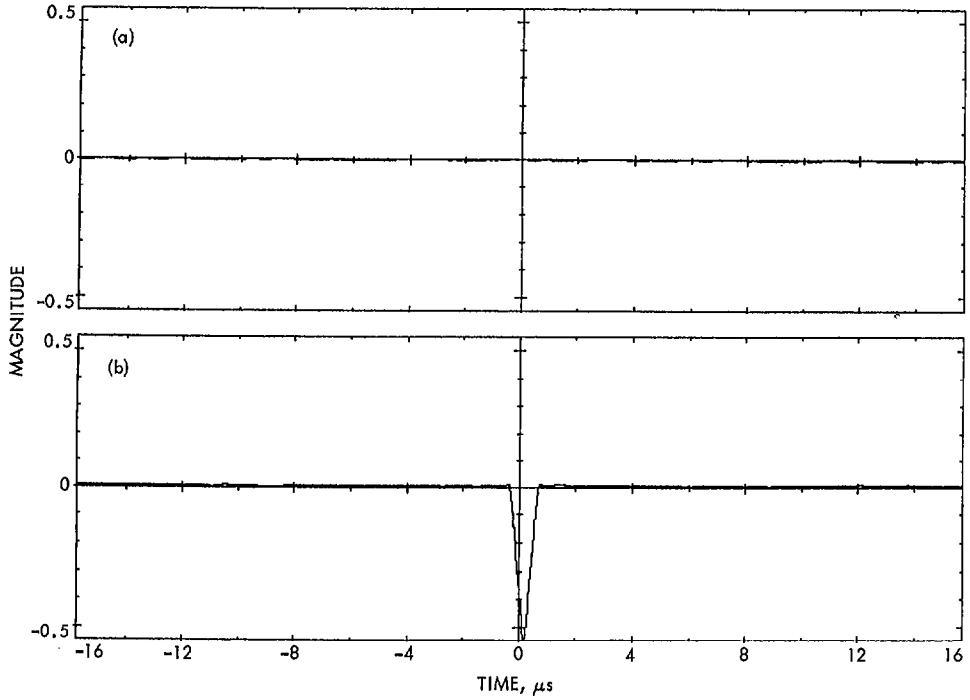

Fig. 13. Cross correlation functions, averaged 16 times: (a) real channel, cross correlation; (b) imaginary channel, cross correlation